Computers Math. Applic. Vol. 26, No. 9, pp. 53–65, 1993
Printed in Great Britain.

0898-1221/93 $6.00 + 0.00

Biorheological Aspects of Arterial Flow Near Bifurcations

J. C. MISRA, M. K. PATRA AND S. C. MISRA*
Department of Mathematics
Indian Institute of Technology, Kharagpur 721302, India

(Received and accepted October 1992)

Abstract—The manner in which the steady flow of a low viscous fluid (representing blood) divides at a junction (where a straight single branch leaves the straight parent trunk) is numerically investigated by adopting conformal mapping techniques in terms of the significant dimensionless parameters: the entrance flow rate index p, the branch diameter ratio β, and the angle of branching α. The ratio of the flow rate in the side branch to the flow rate in the main branch, γ, is found to increase with a reduction in the flow index p and with an increase in β. The problem is analyzed by a numerical approach and a visualization technique is employed to establish the existence of two interdependent separation regions, one in each branch. The location of the occurrence of separation and the size of the separated regions are found to be dependent on the value of γ. The study depicts the formation, growth, and shedding of vortices in the separated region of the main branch and the double-helicoidal flow in the side branch.

1. INTRODUCTION

It has been experienced that an accurate knowledge of the geometry of arterial segments is essential in the analysis of both the deformable characteristics and the hemodynamic properties of arteries. In the case of a branched arterial segment or a bifurcation, the geometrical configuration is very complex and the task of understanding the elastic and hemodynamic behaviour in the neighbourhood of the branching presents a formidable challenge. In its native environment, blood flows through a series of bifurcations as it courses its way through the vascular network. Flow through branched tubes has been of particular interest, in view of the possibility that characteristics of the flow may be related to certain forms of arterial disease. Since diseases and defects of the human cardiovascular system remain an important cause of death, researchers are expending considerable energy to understand this complex system. Besides biochemical factors, the hydrodynamic ones play a major role for atherosclerosis, deposition of blood platelets and lipids. Of the various cardiovascular diseases, atherosclerosis is the most frequent one. Deposits and blockages are mostly found at bends and bifurcations of human arteries [1–3]. The flow is changed there and vorticities as well as secondary flows may also occur at these sites. Of greater interest are the stagnation points, the flow separation, the reverse flow, and the reattachment of the flow. The duration for which particles remain in such reverse flow areas is a decisive factor [4]. The geometry of the bifurcation has an influence over the location of the flow separation, but the flow rate is of no less importance.

General studies have presented steady and pulsatile profiles of velocity in branched tubes with a branch-to-trunk area ratio greater than one [5,6]. Kuchar and Ostrach [7] considered entrance effects associated with laminar flows of viscous fluids in uniformly circular cylindrical

*Present address: Department of Electronics and Communication Engineering, Andhra University College of Engineering, Visakhapatnam 530003, India.

elastic tubes. The problem becomes more complex in the case of branched vessels. Martin and Clark [8] experimentally and theoretically analyzed wave reflections in branched flexible conduits. Malindzak [9] subsequently made more sophisticated *in-vivo* analyses of the wave reflections. An experimental study was conducted by Matsuo and Okeda [10] to investigate the hydrodynamics of branching flow in relation to the blood supply to the basal part of the brain. It was revealed that in the blood circulation, branching loss is important where a small artery divides off with a large branching angle from a large trunk. Liepsch [11] studied the flow behaviour (like separation, stagnation, and reattachment points) in bends and bifurcations of arterial models, involving steady and pulsatile flow conditions in rigid and elastic models with Newtonian and non-Newtonian fluids. He showed that the flow can be optimized in such a manner as to minimize the pressure drop. This means that no additional pressure loss due to separation or turbulence should occur, since such losses increase the pumping power requirements.

Roach *et al.* [12] used a dye to study the flow in glass models of arterial bifurcations. They have emphasized the importance of bifurcation geometry and of possible changes in the bifurcation geometry in understanding cerebral vascular hemodynamics. Roach [13] pointed out the lack of mapping techniques for lesions near the apex of bifurcations. Schneck and Gutstein [14] observed some correlation between the occurrence of the atherosclerotic plaques and the angle of bending and branching. Rodkiewicz and Howell [15] studied the manner in which the flow divides at an arterial bifurcation as a function of the significant dimensionless parameters: Reynolds number, unsteadiness parameters, and velocity function parameter. They found that for certain values of these parameters, more fluid flows into the side branch. This led to the important conclusion that for a bifurcation in a rigid wall, the blood flow generating system, activated by an impulse from the brain, could supply more blood to the preferential area of the human body by changing the values of these three parameters. Murray [16] studied the relation between the weight of a branch of a tree, its diameter, and its branching angle. He showed that the circumference of a branch is related to the total weight distal to it by a power function: Weight $= 7.08\,(\text{circumference})^{2.49}$. In a separate communication [17], he showed that in a blood vessel with laminar flow, when minimal power is being used to move the blood, flow $\propto$ (radius)^3. Uylings [18] developed the concept further and showed that at the optimum, flow $\propto$ (radius)$^{(j+2)/(j-2)}$, where j has the value 4 for laminar flow, 5 for turbulent flow, and intermediate values for transitional flow regimes.

For arterial branching in the cardiovascular system, the dominant mode is that in which a single stream of blood divides into two separate streams. The two branch streams may vary considerably in their relative size and direction, but the underlying functional phenomenon is the same as when a stream of blood is divided into two separate streams. In the study of vascular anatomy, a distinction is generally made between a branching side at which a parent artery divides into two nearly equal branches and one in which the parent artery gives off a relatively small branch. The rather rare case, in which the two branch streams are equal, shall be referred to as a symmetrical bifurcation. The complex flow pattern at the bifurcation of a stream makes a complete analysis of the problem nearly impossible. However, by adopting the conformal mapping technique, the complex nature of three-dimensional flows in the case of arterial branching has been demonstrated here.

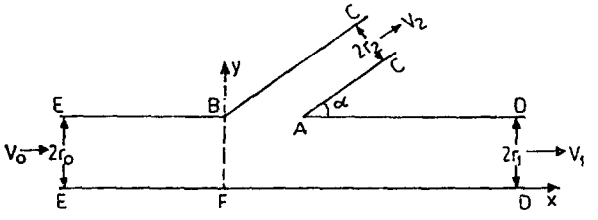

Figure 1a. Schematic diagram of the horizontal cross-section (in the z-plane) of the arterial segment having a bifurcation.

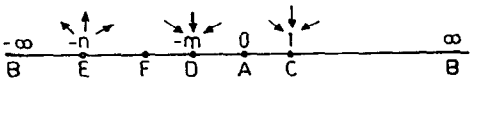

Figure 1b. ζ-plane.

The present paper deals with an analysis of blood flow in arterial bifurcations. The analysis has been carried out analytically by using the conformal mapping approach. The branched artery has been modelled as a circular tube having a circularly cylindrical branch. The analysis performs in the situation where a single stream divides into two separate streams. Numerical computations for a specific case reveal several very important aspects of arterial flow near bifurcations.

2. PROBLEM FORMULATION AND TECHNICAL ASSUMPTIONS

Let us consider a nonsymmetrical bifurcation in an arterial segment (having circular cross-section), which consists of a parent artery and two daughter branches of unequal diameters. Here, the vascular bed has been considered horizontal. Figure 1a shows the horizontal cross-section through the axes of the arterial segments. The analysis has been performed on the basis of the following simplifying assumptions:

(i) The flow energy is supplied only at the beginning of the system, and there are no energy sinks in the system due to bifurcation or, if present, it takes place downstream of the junction.
(ii) The flow is steady and axisymmetric.
(iii) Blood may be treated as a homogeneous fluid with low viscosity.
(iv) The walls of the channel are considered to be rigid.

3. METHOD OF SOLUTION

The problem will be analyzed here by employing the method of conformal mapping, by considering the viscosity of blood to be small. In Figure 1a, EFDDACCBE represents schematically the geometrical configuration of the boundaries of a section of the arterial bifurcation. F is taken as origin and the axes of x and y are chosen along FD and FB, respectively, in the z-plane. α denotes the angle of bifurcation CAD. The boundaries of the arterial wall segment are taken to be straight.

By using the Schwarz-Christoffel theorem, the various boundaries of the arterial junction (cf. Figure 1a) may be transformed to the real axis of a ζ-plane (cf. Figure 1b), and the region of flow between the boundaries is transferred to the upper half of the ζ-plane.

Referring to Figure 1b, the expression for the transformation function is given by

$$\frac{dz}{d\zeta} = \frac{-K\,\zeta^{1-\alpha/\pi}}{(\zeta+n)\,(\zeta+m)\,(\zeta-1)} \tag{1}$$

$$= K\,\zeta^{-\alpha/\pi}\left[\frac{n}{(n-m)\,(1+n)}\,\frac{1}{\zeta+n} - \frac{m}{(n-m)\,(1+m)}\,\frac{1}{\zeta+m} - \frac{1}{(1+m)\,(1+n)}\,\frac{1}{\zeta-1}\right], \tag{2}$$

in which K is a complex constant and m, n are real unknowns that represent, respectively, the distances AD and AE. m and n have been calculated at a later stage.

Throughout this study, a subscript 0 shall be used to refer to the parent artery, subscript 1 to the larger of the two daughter branches, and subscript 2 to the smaller branch.

With F as origin in the z-plane and using the standard results of integration [19], the integration of equation (2) between A and B (cf. Figure 1a) yields

$$\begin{aligned} 2r_2 \csc\alpha - 2\,(r_0 - r_1)\,\cot\alpha - 2i\,(r_0 - r_1) \\ = K\left[\frac{n}{(n-m)(1+n)}\int_{\infty}^{0}\frac{\zeta^{-\alpha/\pi}}{\zeta+n}\,d\zeta - \frac{m}{(n-m)(1+m)}\int_{\infty}^{0}\frac{\zeta^{-\alpha/\pi}}{\zeta+m}\,d\zeta\right. \\ \left. -\frac{1}{(1+m)\,(1+n)}\int_{-\infty}^{0}\frac{\zeta^{-\alpha/\pi}}{\zeta-1}\,d\zeta\right] \\ = \frac{K\pi}{\sin\alpha}\left[\frac{m^{1-\alpha/\pi}}{(n-m)\,(1+m)} - \frac{n^{1-\alpha/\pi}}{(n-m)\,(1+n)} + \frac{\cos\alpha - i\sin\alpha}{(1+m)\,(1+n)}\right]; \qquad 0<\alpha<\pi, \end{aligned} \tag{3}$$

in which r denotes the uniform radius of an artery. Assuming $K = K_1 + i K_2$ in (3) and separating the real and imaginary quantities, we have

$$2r_2 \csc\alpha - 2(r_0 - r_1)\cot\alpha = \frac{K_1\pi}{\sin\alpha}\left[\frac{m^{1-\alpha/\pi}}{(n-m)(1+m)} - \frac{n^{1-\alpha/\pi}}{(n-m)(1+n)} + \frac{\cos\alpha}{(1+m)(1+n)}\right] + \frac{K_2\pi}{(1+m)(1+n)}, \quad \text{and} \tag{4}$$

$$2(r_0 - r_1) = \frac{K_2\pi}{\sin\alpha}\left[\frac{n^{1-\alpha/\pi}}{(n-m)(1+n)} - \frac{m^{1-\alpha/\pi}}{(n-m)(1+m)} - \frac{\cos\alpha}{(1+m)(1+n)}\right] + \frac{K_1\pi}{(1+m)(1+n)}. \tag{5}$$

Further integrating equation (2) separately in a small interval $[-m-\varepsilon, -m+\varepsilon]$ for the point D, and $[-n-\varepsilon, -n+\epsilon]$ for the point E in the ζ-plane, we get

$$\begin{aligned} r_1 &= \frac{\pi m^{1-\alpha/\pi}(K_1\cos\alpha + K_2\sin\alpha)}{2(n-m)(1+m)}, \quad \text{and} \\ r_0 &= \frac{\pi n^{1-\alpha/\pi}(K_1\cos\alpha + K_2\sin\alpha)}{2(n-m)(1+n)}. \end{aligned} \tag{6}$$

For $r_1 = r_0$, we have from (6),

$$\frac{m^{1-\alpha/\pi}}{1+m} = \frac{n^{1-\alpha/\pi}}{1+n}, \tag{7}$$

and with the help of (7), we get from (4) and (5), respectively,

$$r_2 = \frac{\pi}{2(1+m)(1+n)}(K_1\cos\alpha + K_2\sin\alpha), \quad \text{and} \tag{8}$$

$$K_1\sin\alpha = K_2\cos\alpha. \tag{9}$$

Using (9), the following simplifications can be made from (6) and (8):

$$r_0 = \frac{K_1\pi n^{1-\alpha/\pi}\sec\alpha}{2(n-m)(1+n)}, \quad r_1 = \frac{K_1\pi m^{1-\alpha/\pi}\sec\alpha}{2(n-m)(1+m)}, \quad \text{and} \quad r_2 = \frac{K_1\pi\sec\alpha}{2(1+m)(1+n)}. \tag{10}$$

These expressions may be used to calculate the unknown quantities, *viz.* m, n, K_1, and K_2 for a given set of values of r_0, r_1, r_2, and α.

As shown in Figure 1b, if in the ζ-plane, two sinks, one each at the points C and D of strengths $V_2 r_2^2$ and $V_1 r_1^2$, respectively, and a source at E of strength $V_0 r_0^2$ are considered, the complex potential in the ζ-plane takes the form

$$w = -V_0 r_0^2 \ln(\zeta + n) + V_1 r_1^2 \ln(\zeta + m) + V_2 r_2^2 \ln(\zeta - 1), \tag{11}$$

in which V denotes the average flow velocity in an artery. If f denotes the flow flux in an artery, then

$$f = \pi r^2 V. \tag{12}$$

Also, the flow balance equation in a bifurcation asserts $f_0 = f_1 + f_2$. Thus, we have

$$V_0 r_0^2 = V_1 r_1^2 + V_2 r_2^2. \tag{13}$$

Now, from (11) and (13), we get

$$\frac{dw}{d\zeta} = -\frac{V_1 r_1^2 + V_2 r_2^2}{\zeta + n} + \frac{V_1 r_1^2}{\zeta + m} + \frac{V_2 r_2^2}{\zeta - 1}, \tag{14}$$

from which the expression for the velocity at any point is obtained as

$$\frac{dw}{dz} = \frac{dw}{d\zeta}\Big/\frac{dz}{d\zeta} = -V_x + iV_y$$
$$= \frac{V_1 r_1^2 + V_2 r_2^2}{K\zeta^{1-\alpha/\pi}}(\zeta+m)(\zeta-1) - \frac{V_1 r_1^2(\zeta+n)(\zeta-1)}{K\zeta^{1-\alpha/\pi}} - \frac{V_2 r_2^2(\zeta+n)(\zeta+m)}{K\zeta^{1-\alpha/\pi}}, \tag{15}$$

in which V_x and V_y are the velocity components in the x and y directions, respectively. For the stagnation point, we must have

$$(V_1 r_1^2 + V_2 r_2^2)(\zeta+m)(\zeta-1) - V_1 r_1^2(\zeta+n)(\zeta-1) - V_2 r_2^2(\zeta+n)(\zeta+m) = 0$$
$$\therefore \zeta = \frac{(n-m)V_1 r_1^2 - m(1+n)V_2 r_2^2}{(n-m)V_1 r_1^2 + (1+n)V_2 r_2^2}. \tag{16}$$

Introducing the results put forward by Uylings [18], $f \propto r^{(j+2)/(j-2)}$ or

$$f = Lr^p, \tag{17}$$

(L being the proportional constant), where j has the value of 4 for laminar flow, 5 for turbulent flow, and intermediate values for transitional flow regimes. Thus, for laminar flow $p = 3$, for turbulent flow $p = 2.\bar{3}$, and for intermediate flow regimes, the value of p could be expected to lie somewhere between $2.\bar{3}$ and 3. Fully turbulent flow, however, may not be developed in the arteries.

Using (12) and (17), we get $V_1/V_2 = (r_1/r_2)^{p-2}$. Thus, equation (16) becomes

$$\zeta = \frac{(n-m) - m(1+n)\beta^p}{(n-m) + (1+n)\beta^p}, \tag{18}$$

where $\beta = r_2/r_1$ represents the ratio of the branch diameters. From equation (18), the position of the stagnation point may be located in the ζ-plane. For different values of α and β, m and n are different. So the value of ζ corresponding to the stagnation point depends on the flow rate. In other words, as p changes its value, the stagnation point moves along the boundary DAC and, correspondingly, the value of ζ lies between $-m$ and 1. When the stagnation point lies on the boundary DA, ζ varies from $-m$ to 0, and when it lies on the boundary AC, ζ varies from 0 to 1. The stagnation point coincides with the corner A when $\zeta = 0$, corresponding to which the value of p may be considered as critical, *viz.* p_{cr}, which is obtained from (18) as

$$p_{cr} = \frac{\ln(n-m) - \ln(m(1+n))}{\ln\beta}. \tag{19}$$

In order to locate the stagnation point in the z-plane, equation (1) may be integrated along AC and AD, which for $r_0 = r_1$ gives

$$\int_{2(r_2\csc\alpha + ir_1)}^{z} dz = K\int_0^{\zeta} \frac{\zeta^{1-\alpha/\pi}}{(\zeta+n)(\zeta+m)(1-\zeta)}\,d\zeta, \tag{20}$$

in which $-m < \zeta < 1$.

4. NUMERICAL APPROACH

The derived analytical expressions have been computed numerically with the purpose of illustrating the applicability of the analysis presented in this paper. In order to examine the influence of the angle of bifurcation, computations have been carried out for five different values

Table 1. Values of ζ and z given by equations (18) and (20) for different x and α.

	p	ζ	z
$\alpha = 15°$	3.0	0.6515	0.4229026
$m = 2.0966$	2.9	0.6294	0.4007336
$n = 213.6112$	2.8	0.6062	0.3786493
$\|K\| = 211.53594$	2.7	0.5818	0.3565861
$p_{cr} = 1.089$	2.6	0.5561	0.3344806
	2.5	0.5291	0.3123751
	2.4	0.5007	0.2902273
$\alpha = 30°$	3.0	0.6292	0.4228376
$m = 1.8747$	2.9	0.6063	0.4003727
$n = 17.4438$	2.8	0.5821	0.3777678
$\|K\| = 16.876917$	2.7	0.5567	0.3551494
$p_{cr} = 1.1511$	2.6	0.5301	0.3325394
	2.5	0.5022	0.3098720
	2.4	0.4731	0.2872383
$\alpha = 45°$	3.0	0.6106	0.4490159
$m = 1.4885$	2.9	0.5873	0.4257418
$n = 6.6285$	2.8	0.5628	0.4023003
$\|K\| = 6.04256$	2.7	0.5373	0.3788944
$p_{cr} = 1.1435$	2.6	0.5106	0.3553448
	2.5	0.4828	0.3317443
	2.4	0.4538	0.3050074
$\alpha = 60°$	3.0	0.6011	0.5013746
m =1.1326	2.9	0.5781	0.4771510
$n = 3.6691$	2.8	0.5542	0.4528799
$\|K\| = 3.169386$	2.7	0.5292	0.4283520
$p_{cr} = 1.0599$	2.6	0.5033	0.4037607
	2.5	0.4764	0.3789888
	2.4	0.4486	0.3541123
$\alpha = 75°$	3.0	0.6011	0.5843919
$m = 0.8419$	2.9	0.5791	0.5593622
$n = 2.3626$	2.8	0.5561	0.5085202
$\|K\| = 1.97146$	2.7	0.5324	0.4913922
$p_{cr} = 0.8966$	2.6	0.5078	0.4827769
	2.5	0.4824	0.4568167
	2.4	0.4562	0.4306003

of $\alpha = 15°$, $30°$, $45°$, $60°$, and $75°$, while $\beta = 0.5$. For each of these cases, the flow behaviour has been studied with different flow rates by considering $p = 3, 2.9, \ldots, 2.4$. The value of β has been extended from its physiological range, for better understanding of the problem and for a possible use in non-physiological cases. In order to obtain the distance of the stagnation point in the z-plane, the right hand side of (20) has been integrated numerically by using Simpson's one-third rule, and the computed results are presented in Table 1.

The diameter of the parent artery and the larger of the daughter branches are considered to be equal to 2 units, whereas the diameter of the smaller of the daughter branches is considered to be 1 unit. For the numerical calculations, the flow region is taken to be finite, and the upstream end of the main channel is considered to be at a distance equal to its radius, the downstream end of the larger daughter branch at a distance equal to thrice its radius, and the smaller branch at a distance of 5 times its radius. The length of the branching region is geometrically determined by the angle of bifurcation α and the width of the branched channel. Furthermore, it is assumed that

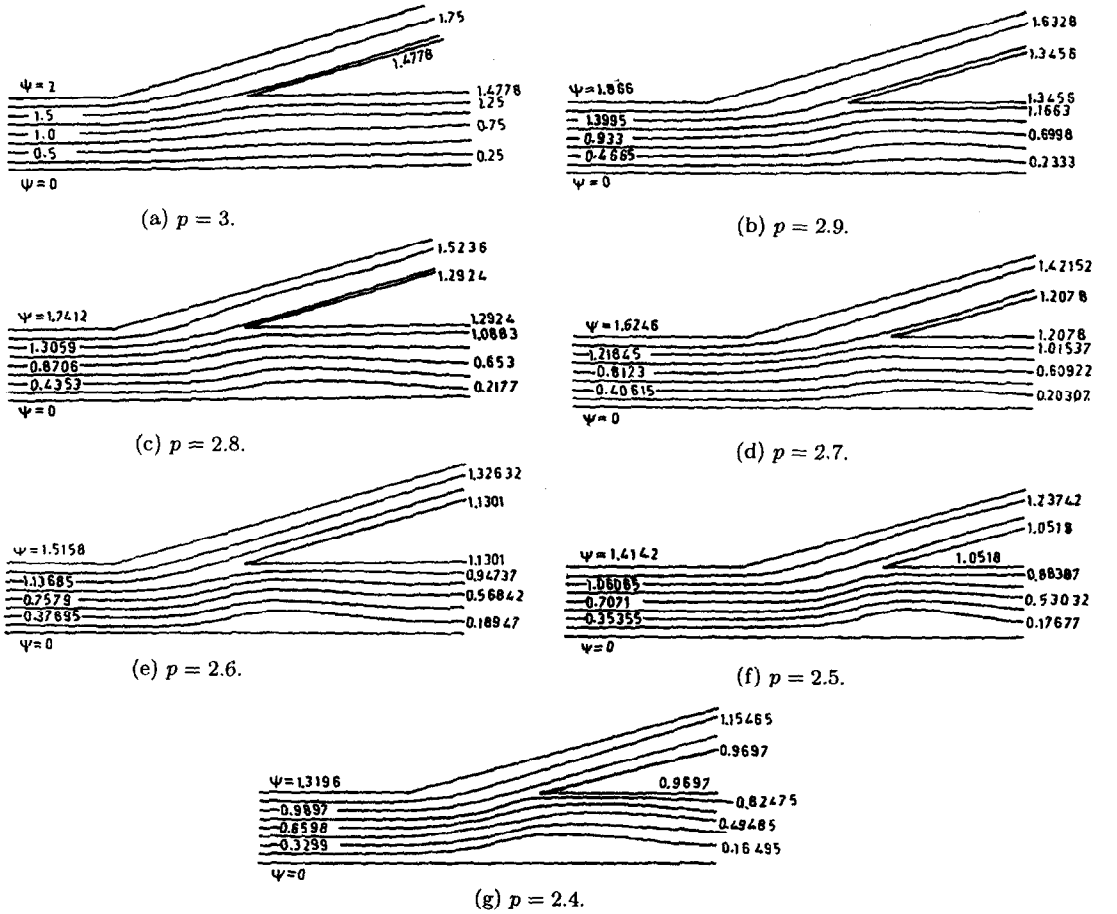

(a) $p = 3$. (b) $p = 2.9$.

(c) $p = 2.8$. (d) $p = 2.7$.

(e) $p = 2.6$. (f) $p = 2.5$.

(g) $p = 2.4$.

Figure 2. Streamlines for $\alpha = 15°$.

when $p = 3$, the average velocity of blood in the entrance region is V_0. Using the numerical results for the steady flow corresponding to the aforementioned values of α and p, streamlines have been drawn (cf. Figures 2–6) to indicate the relative importance of flow rate upon flow paths.

To find the streamlines within the domain bounded by EFDDACCBE, the loci characterized by Ψ = a constant must be found, which is the information obtained by solving $\frac{\partial^2 \Psi}{\partial x^2} + \frac{\partial^2 \Psi}{\partial y^2} = 0$, subject to values of Ψ specified on the boundaries. BC, AC, and AD are obviously streamlines, since the velocity is along the tangent to these lines. The value $\Psi = 0$ is assigned to the segment ED, since it is only necessary to know the value of the stream function to the extent of an additive constant. The values of Ψ along EBC, AC, and AD can be found from the relations $V_x = -\frac{\partial \Psi}{\partial y}$, $V_y = \frac{\partial \Psi}{\partial x}$ and from the geometrical configuration of the model. The value of the stream function is now known at all the points on the boundary, and it remains to satisfy Laplace's equation within these boundaries. The partial derivatives in this equation may be approximated by Taylor's theorem (cf. [20]) for a function of two variables. The theorem gives

$$\begin{aligned}\Psi(x+h, y+k) = \Psi(x,y) &+ \left(h\frac{\partial \Psi}{\partial x} + k\frac{\partial \Psi}{\partial y}\right) + \frac{1}{2!}\left(h^2\frac{\partial^2 \Psi}{\partial x^2} + 2hk\frac{\partial^2 \Psi}{\partial x\,\partial y} + k^2\frac{\partial^2 \Psi}{\partial y^2}\right) \\ &+ \frac{1}{3!}\left(h^3\frac{\partial^3 \Psi}{\partial x^3} + 3h^2k\frac{\partial^3 \Psi}{\partial x^2\,\partial y} + 3hk^2\frac{\partial^3 \Psi}{\partial x \partial y^2} + k^3\frac{\partial^3 \Psi}{\partial y^3}\right) \\ &+ \frac{1}{4!}\left(h^4\frac{\partial^4 \Psi}{\partial x^4} + 4h^3k\frac{\partial^4 \Psi}{\partial x^3\,\partial y} + 6h^2k^2\frac{\partial^4 \Psi}{\partial x^2 \partial y^2} + 4hk^3\frac{\partial^4 \Psi}{\partial x\,\partial y^3} + k^4\frac{\partial^4 \Psi}{\partial y^4}\right) + \cdots,\end{aligned} \tag{21}$$

and it is assumed that the partial derivatives of Ψ are continuous up to an order required by the

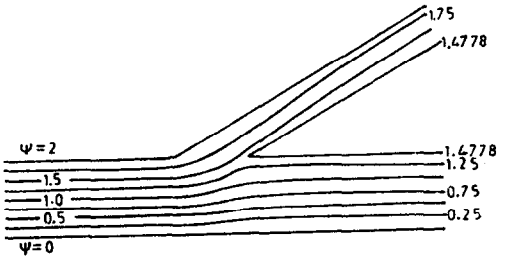

(a) $p = 3$.

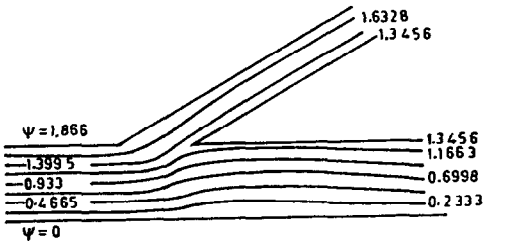

(b) $p = 2.9$.

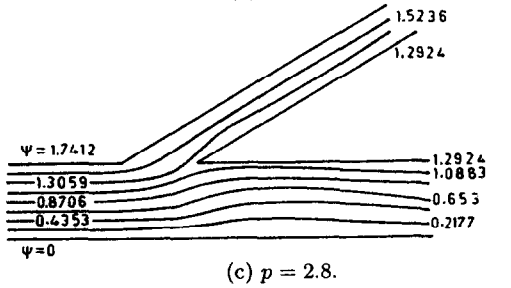

(c) $p = 2.8$.

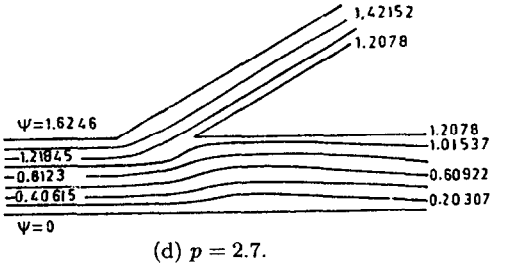

(d) $p = 2.7$.

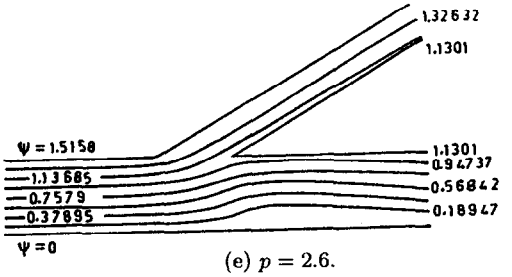

(e) $p = 2.6$.

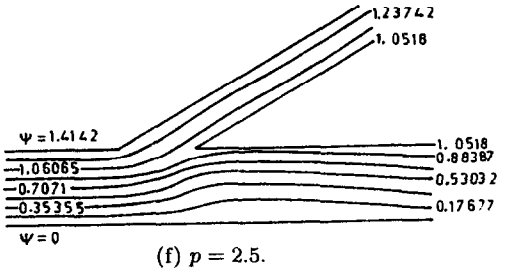

(f) $p = 2.5$.

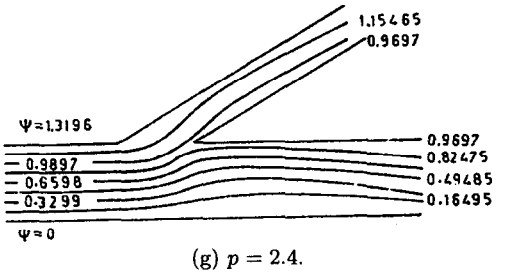

(g) $p = 2.4$.

Figure 3. Streamlines for $\alpha = 30°$.

accuracy of representation of the function. Equation (21) may be used to approximate both $\frac{\partial^2 \Psi}{\partial x^2}$ and $\frac{\partial^2 \Psi}{\partial y^2}$, for example, with $k = 0$,

$$\Psi(x+h,y) = \Psi(x,y) + h\frac{\partial \Psi}{\partial x} + \frac{h^2}{2!}\frac{\partial^2 \Psi}{\partial x^2} + \frac{h^3}{3!}\frac{\partial^3 \Psi}{\partial x^3} + \frac{h^4}{4!}\frac{\partial^4 \Psi}{\partial x^4} + \cdots, \quad \text{and} \tag{22}$$

$$\Psi(x-h,y) = \Psi(x,y) - h\frac{\partial \Psi}{\partial x} + \frac{h^2}{2!}\frac{\partial^2 \Psi}{\partial x^2} - \frac{h^3}{3!}\frac{\partial^3 \Psi}{\partial x^3} + \frac{h^4}{4!}\frac{\partial^4 \Psi}{\partial x^4} - \cdots. \tag{23}$$

Adding (22) and (23), one obtains

$$\Psi(x+h,y) + \Psi(x-h,y) = 2\Psi(x,y) + \frac{2h^2}{2!}\frac{\partial^2 \Psi}{\partial x^2} + \frac{2h^4}{4!}\frac{\partial^4 \Psi}{\partial x^4} + \cdots.$$

If h^2 is large compared to h^4, by making h suitably small, we can write

$$\frac{\partial^2 \Psi}{\partial x^2} \approx \frac{\Psi(x+h,y) + \Psi(x-h,y) - 2\Psi(x,y)}{h^2}.$$

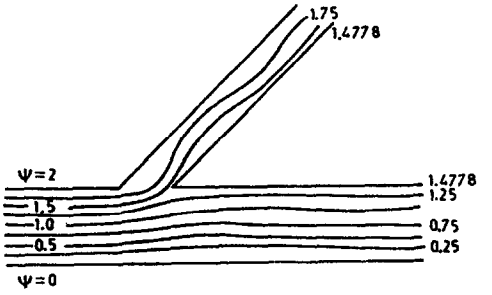

(a) $p = 3$.

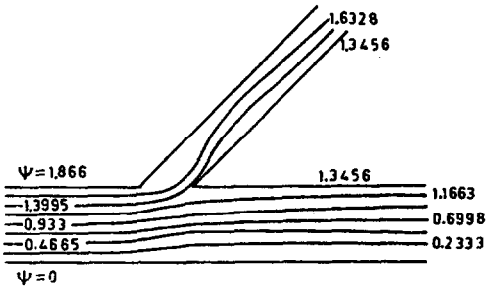

(b) $p = 2.9$.

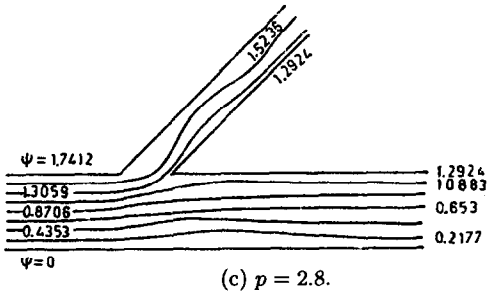

(c) $p = 2.8$.

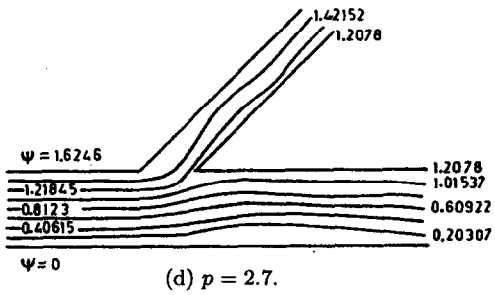

(d) $p = 2.7$.

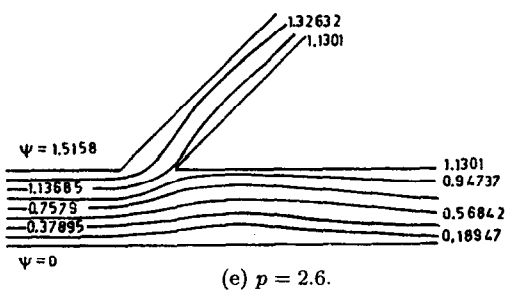

(e) $p = 2.6$.

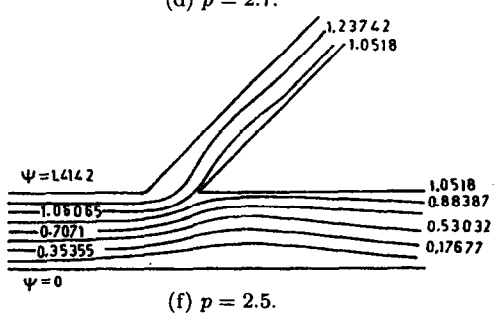

(f) $p = 2.5$.

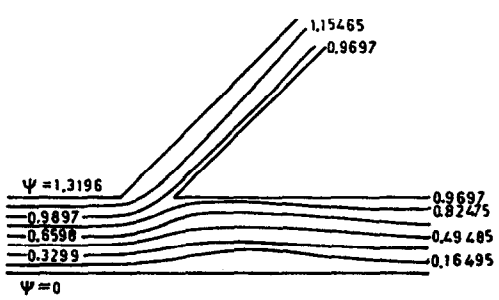

(g) $p = 2.4$.

Figure 4. Streamlines for $\alpha = 45°$.

Similarly,

$$\frac{\partial^2 \Psi}{\partial y^2} \approx \frac{\Psi(x, y+k) + \Psi(x, y-k) - 2\Psi(x, y)}{k^2},$$

when k^2 is large compared to k^4. To satisfy the equation $\frac{\partial^2 \Psi}{\partial x^2} + \frac{\partial^2 \Psi}{\partial y^2} = 0$, setting $k = h$, we have

$$\Psi(x+h, y) + \Psi(x-h, y) + \Psi(x, y+h) + \Psi(x, y-h) - 4\Psi(x, y) = 0. \tag{24}$$

This equation must be satisfied at points within the domain of the solution of Laplace's equation. For further work, the interval $0 \leq y \leq 2$ is divided into 16 equal intervals. Taking $h = 1/8$, we form a square net on the z-plane. The node at $(x = ih,\ y = jh)$ is designated the ij-node, $i = \ldots, -2, -1, 0, 1, 2, \ldots$; $j = 0, 1, 2, \ldots, 16$. For the ij-node, we have the relation

$$\Psi_{i+h,j} + \Psi_{i-h,j} + \Psi_{i,j+h} + \Psi_{i,j-h} - 4\Psi_{ij} = 0. \tag{25}$$

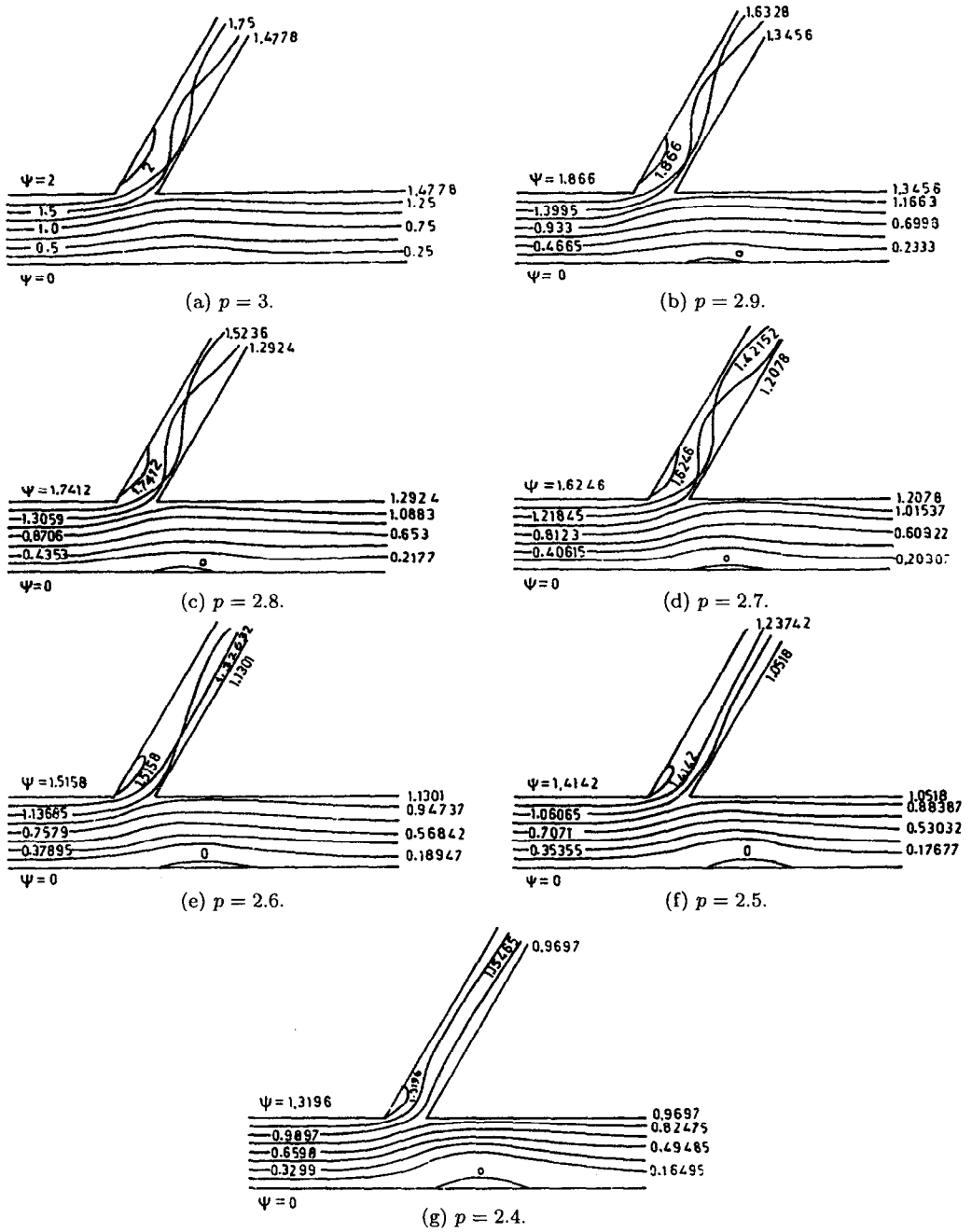

Figure 5. Streamlines for $\alpha = 60°$.

For each interior node, we can obtain a relation similar to (25) involving the stream function Ψ. We thus have a large number of similtaneous equations involving the same number of unknown variables Ψ at each of the nodes. These simultaneous field equations have been solved by the matrix inversion method, by using a high speed computer. After calculating the nodal values of the stream function at each node, the streamlines have been drawn by using the method of interpolation.

5. RESULTS AND DISCUSSION

From the figures, one may note that there is a change in the streamline patterns with increase in the flow rate (Reynolds number). At higher flow rates, streamlines are more distinctly displaced

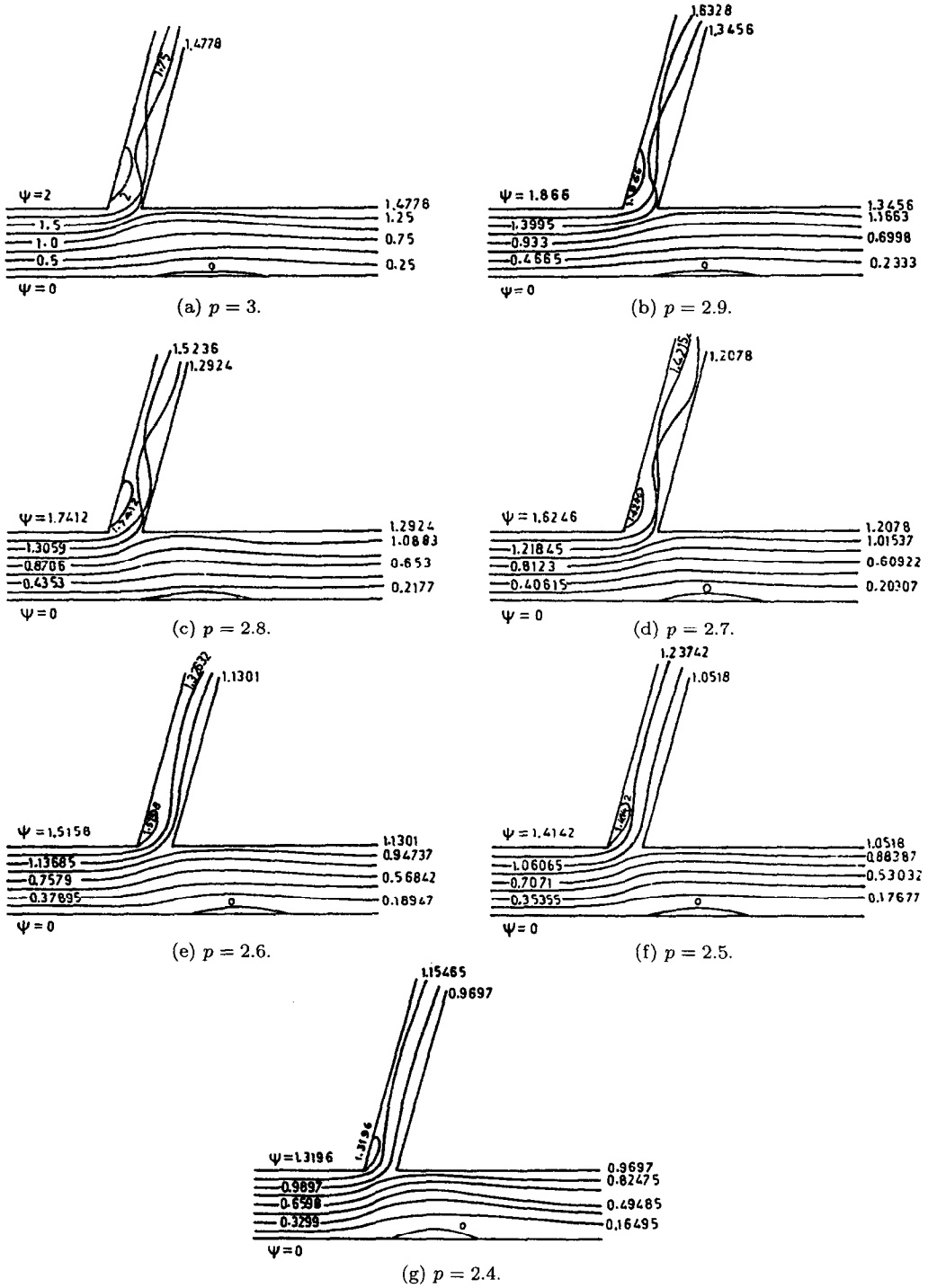

Figure 6. Streamlines for $\alpha = 75°$.

towards the flow divider than those at lower flow rates; the deviation from the axial direction is found to be largest for least flow rate, for a given upstream velocity. The separation region grows in the main branch when the flow rate decreases and also when the angle of branching is not less than 60°. Results indicate further that when the separation region in the main branch increases, the separation region in the side branch decreases, and vice versa. Inside the separation regions, vortices are generated. The streamlines on the wall, except in this region in the main branch, run smoothly downstream. It is to be noted that standing vortex is not seen downstream of the corner

for $\alpha = 15°$, 30°, and 45°, but it appears in the side branch for the other cases, and it becomes larger as the angle of bifurcation α increases. For the cases $\alpha = 60°$ and 75°, another standing vortex is seen on the straight branch (cf. Figures 5 and 6). The vortex point of the bifurcating streamline becomes closer to the corner as the angle of branching increases. It is further observed from the figures that the size of the vortex in the straight branch increases when the vortex in the side branch decreases, and vice versa. Inside the side branch, the flow becomes double-helicoidal, which is typical of flows in curved pipes. The stagnation point of the bifurcating streamline is nearer to the corner for $\alpha = 30°$ than for $\alpha = 15°$, but it is at an increasing distance from the corner, for $\alpha = 45°$, 60°, and 75°. From Table 1, it may be observed that as the flow rate in the main channel as well as the branching angle increases, the stagnation point of the bifurcating streamline moves downstream to the corner. Also, the crititical value of the flow rate index p decreases as the angle of branching increases, except for the case when $\alpha = 15°$.

The dependence of the mass flow ratio γ (ratio of the flow rate in the side branch to the flow rate in the main branch) on the flow rate in the mother trunk is exhibited in Figure 7. This graph shows that γ decreases with the increase in the flow rate in the main tube. This could be attributed to the inability of the fluid to negotiate the turn, due to an increase of its momentum in the main-line direction. The change in γ is due to a variation in size and location of two interdependent (one in the main branch and the other in the side branch) separation regions. Since growth of the separation region in the main branch restricts the flow in this branch, the mass flow ratio increases.

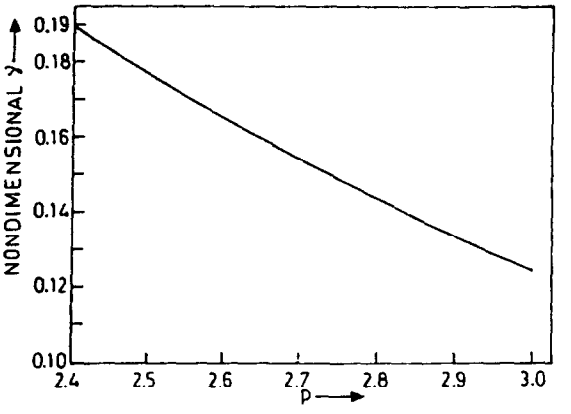

Figure 7. Mass flow ratio versus flow rate.

Our results are in conformity to the experimental observations made by Lutz *et al.* [21] that as the flow proceeds downstream from the entrance, the profiles become progressively more skewed towards the ventral side (branch side) of the model. This effect seems to be more pronounced as the daughter branch flow is increased and as one proceeds farther downstream. As a result, the wall velocity gradient on the dorsal wall (opposite the branches) decreases, resulting in lower shear rates there. Eventually, a point of flow separation and flow reversal is detected on the dorsal wall. It may be pointed out that both in the present case and in the aforesaid experimental study, the model considered is rigid, not flexible. The separation on the outer wall of a daughter branch can be eliminated by increasing the flow rate to the branch, keeping the main flow Reynolds number fixed. These findings agree with our results. Our results also agree with those of Karino and Goldsmith [22] who investigated the effects of branch angle on flow phenomena in models, and reported that vortex formation on the outer wall of a daughter branch occurs at lower values of the branch flow ratio as the angle of the daughter branch increases.

REFERENCES

1. C.G. Caro, Arterial fluid mechanics and atherogenesis, *Recent Adv. in Cardiov. Disease* **11** (1), 6–11 (1981).
2. R.J. Pedley, *The Fluid Mechanics of Large Blood Vessels*, Cambridge University Press, New York, (1979).
3. G. Schettler, R.M. Nerem, H. Schmid-Schönbein, H. Mörle and C. Diehm (Editors), *Fluid Dynamics as a Localizing Factor for Atherosclerosis*, Springer-Verlag, Berlin, (1983).
4. H. Goldsmith and T. Karino, Microheology and clinical medicine: Unravelling some problems related to thrombosis, *Recent Adv. in Cardiov. Disease* **11** (1), Supplement 40–52 (1981).
5. K. Kandarpa and N. Davids, Analysis of the fluid dynamic effects on atherogenesis at branching sites, *J. Biomech.* **9** (11), 735–741 (1976).
6. A.I. Feuerstein, O.A. Ei Masry and G.F. Round, Arterial bifurcation flows—Effects of flow rate and area ratio, *Can. J. Physiol. Pharmacol.* **54**, 795–808 (1976).
7. N.R. Kuchar and S. Ostrach, Flows in the entrance regions of circular elastic tubes, Case Western Reserve University Publication No. FTAS/TR-65-3, Cleveland, OH, (1965).
8. J.D. Martin and M.E. Clark, Theoretical and experimental analyses of wave reflections in branched flexible conduits, *TRA/ASCE* **131**, 441–457 (1966).
9. G.S. Malindzak, Reflection of pressure pulses in the aorta, *Medical Res. Engng.* **6** (4), 25–31 (1967).
10. T. Matsuo and R. Okeda, Hydrodynamics of arterial branching—The effect of arterial branching on distal blood supply, *Biorheol.* **26** (6), 799–811 (1989).
11. D.W. Liepsch, Flow in tubes and arteries—A comparison, *Biorheol.* **23** (4), 395–433 (1986).
12. M.R. Roach, S. Scott and G.F. Ferguson, Hemodynamic importance of the geometry of bifurcations in the circle of Willis (Glass model studies), *Stroke* **3**, 255–267 (1972).
13. M.R. Roach, Biophysical analyses of blood vessel walls and blood flow, *Ann. Rev. Physiol.* **39** (1), 51–71 (1977).
14. D.J. Schneck and W.H. Gutstein, Boundary-layer studies in blood flow, ASME Paper No. 66-WA/BHF-4, (1966).
15. C.M. Rodkiewicz and D.H. Howell, Fluid dynamics in a large arterial bifurcation, *AIAA J* **9** (11), 2284–2286 (1971).
16. C.D. Murray, A relationship between circumference and weight in trees and its bearing on branching angles, *J. Gen. Physiol.* **10**, 725–729 (1927).
17. C.D. Murray, The physiological principle of minimal work, the vascular system and the cost of blood volume, *Proc. Nat. Acad. Sci. USA* **12**, 207–214 (1926).
18. H.B.M. Uylings, Optimization of diameters and bifurcation angles in lung and vascular tree structures, *Bull. Math. Biol* **39** (1), 509–520 (1977).
19. R.V. Churchil and J.W. Brown, *Complex Variables and Applications*, p. 195, McGraw-Hill Publishing Company, New York, (1990).
20. H.K. Crowder and S.W. McCuskey, *Topics in Higher Analysis*, pp. 223–225, The Macmillan Company, New York, (1964).
21. R.J. Lutz, L. Hsu, A. Menawat, J. Zrubek and K. Edwards, Comparison of steady and pulsatile flow in a double branching arterial model, *J. Biomech.* **16** (9), 753–766 (1983).
22. T. Karino and H.L. Goldsmith, Disturbed flow in models of branching vessels, *Trans. Am. Soc. Civ. Engrs.* **26**, 500–505 (1980).